Low-dispersion ultra-high-bandwidth vertical-cavity surface-emitting laser arrays

Stewart T. M. Fryslie*, Kent D. Choquette
University of Illinois at Urbana-Champaign, 208 N Wright St, Champaign, IL, USA 61820

ABSTRACT

We show a novel design and operation technique for an array of optically coupled vertical cavity surface emitting lasers enabling high-performance optical transmission. Bandwidths up to 37 GHz have been obtained under single-mode operation with narrow spectral width and increased output power while the laser array is biased at low current density. Using dynamic coupled mode theory analysis we determine important design parameters to engineer for greater enhancement of modulation response.

Keywords: Vertical cavity laser, semiconductor laser, photonic crystal, modulation bandwidth, phased arrays, semiconductor laser arrays, coherent coupling, injection locking

1. INTRODUCTION

Vertical cavity surface-emitting lasers (VCSELs) possess desirable characteristics such as low power consumption, circular beam output for efficient fiber coupling, low-cost manufacturability, and scalability in two-dimensional arrays. Therefore they have become the dominant source for low-cost, high-performance optical data communication links in computer server, data center, and super computer applications. It has been estimated that more than a billion VCSELs have been deployed to date in commercial applications [1].

As data centers and the like require greater bandwidth and become physically larger in size, there is an ever-increasing demand on the optical interconnect for high data rate over longer fiber transmission distance. There have been several reports of VCSEL modulation rate in excess of 50 Gb/s [2, 3] as high as 72 Gb/s, although these experiments have been into a few 10s of meter of fiber and require excessively high current density operation. Modulation rate times distance products of 25 × 1 [4], 20 × 2 [5], and 1 × 10 [6] Gb/s × km have been reported. To satisfy the need for optical data communications links requiring error-free transmission over longer distances (>1 km) of fiber at higher data rate (>20 Gbps), it is crucial to employ VCSELs with large modulation bandwidth, single mode or narrow spectral width, sufficient output power, and reliable operation.

The integration of a photonic crystal into a conventional VCSEL has shown itself to be a reliable method of creating single-mode lasers [7]. This concept has also been used to create coherently coupled anti-guided microcavity laser arrays [8]. Modulation bandwidth for free-running VCSELs typically ranges from few to twenty GHz. An interesting recent discovery is that modulation bandwidth may be appreciably improved with coherently coupled arrays [9, 10]. Recently we reported the ability to tune 2 × 1 phased, photonic crystal VCSEL arrays into various regions of coherently coupled operation [11] and have shown their utilization for producing greatly enhanced resonance frequency and modulation bandwidth with highly single-mode emission [10, 12, 13]. We have recently reported small signal bandwidth of 37 GHz (receiver limited) with side-mode suppression ratio (SMSR) of 40 dB and narrow RMS spectral width of 0.042 nm for the coherently coupled out-of-phase supermode. Due to the coherent coupling in these arrays, the bandwidth enhancement is accompanied by an increased output power of >3.4 mW and is achieved at an operating current density of <8 kA/cm^2, which is in the regime of high-reliability operation with long device lifetime by industrial standards [14]. Lasers with such performance characteristics may greatly enhance high-rate data transfer in computer server, data center, and supercomputer applications with potentially long device lifetime.

We have also performed large-signal modulation experiments to verify that the arrays are suitable for practical applications. We have applied dynamic coupled mode theory to evaluate relevant aspects of modulation response and locking range dynamics observed from coherently coupled 2x1 arrays [15]. In the following sections we report a summary of our work.

Vertical-Cavity Surface-Emitting Lasers XX, edited by Kent D. Choquette,
James K. Guenter, Proc. of SPIE Vol. 9766, 97660J · © 2016 SPIE
CCC code: 0277-786X/16/$18 · doi: 10.1117/12.2218907

2. METHODOLOGY

2.1 Device Design and Fabrication

A cross-sectional sketch with top-view photo and inset scanning electron microscope image of the 2×1 high-speed photonic crystal VCSEL array are shown in Fig. 3.1 [10, 11]. Standard VCSEL epitaxial material emitting nominally at both the 850 nm and 975 nm wavelengths have been used to fabricate laser arrays for on-chip high speed measurements. The phased coherently coupled VCSEL arrays are fabricated by combining a photonic crystal etched hole pattern that defines the array optical cavity, with an ion implant-defined laser gain structure [8]. Multiple device designs were studied where the photonic crystal parameters subject to variation are hole pitch *a* and hole diameter *b* in either a hexagonal- or square-lattice pattern. The laser elements of the phased array correspond to the two missing holes (lattice defects) in the photonic crystal pattern (see inset Fig. 3.1). To enhance optical coupling between neighboring elements in the array, the photonic crystal is designed such that there is no etched hole directly between array elements and with holes nearest this inter-element coupling region having reduced size. The photonic crystal *a* and *b* parameters used here have enabled single Gaussian mode operation for single element VCSELs by providing an appropriate and stable index guiding with greater optical loss for higher order modes [16, 17].

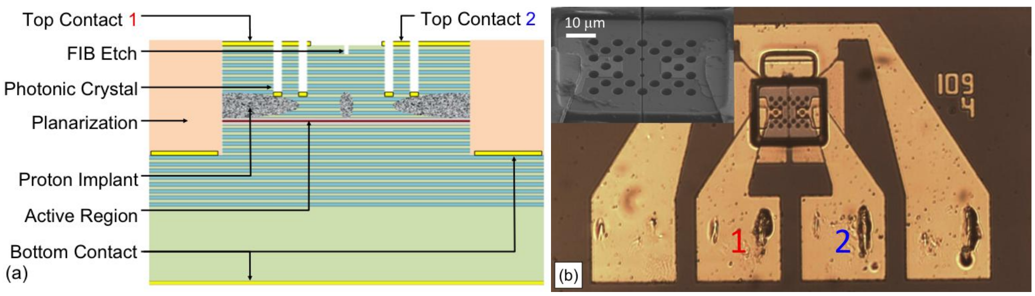

Figure 1. Cross-sectional sketch and top-view image with inset scanning electron micrograph of a 2×1 optically coupled, phased vertical cavity laser array with planarized contacts for high-speed modulation.

The current apertures defined by ion-implantation are designed such that they overlap both a unique top metal contact and the photonic crystal apertures of each element [18]. The current apertures have combined cross section areas between 100 to 140 μm^2 and are separated by ~2 μm of implanted semiconductor between the elements. This structure enables strong optical coupling between array elements and stable coherently coupled operation under proper biasing conditions.

The array fabrication begins with patterning the photonic crystal within a mesa, which we accomplish with the deposition, photolithographic patterning, and reactive-ion etching (RIE) of a SiO_2 mask. Next, gain apertures defined photolithographicaly using a thick photoresist mask are formed by a single high energy (340 keV) proton implantation with dose of 5×10^{14} ions/cm^2. After implantation and resist removal, the photonic crystal and mesa are created simultaneously using inductively coupled plasma reactive ion etching. Next are the depositions of unique p-type ohmic contacts for each array element and common n-type contacts, followed by planarization using HD-4104 polyimide, and deposition of ground-signal-signal-ground coplanar interconnect metal contacts. Planarization helps to avoid stress induced refractive index change while probing the device and reduces the contact pad capacitance which allows for high-speed amplitude modulation of the array [10, 19]. In order to achieve the critical electrical isolation between the array elements, the highly electrically conductive top DBR period is bisected between the array elements and top contacts by focused ion beam etching (FIBE). The post-fabrication FIBE step could be replaced with a stacked multiple ion implantation procedure. Hence the phased VCSEL arrays do not require custom epitaxial layers and rely solely on conventional fabrication processes that have proven to be reliable for single element VCSELs.

2.2 Spectral and Coherence Tuning

The light output versus bias current for the 2×1 VCSEL array is shown in Fig. 2 for different biasing schemes of the two array elements. Fig. 2 shows the array output for an injection current to Element 1 only, Element 2 only, and the total current with equal bias on each element simultaneously. Note that the VCSEL array is an imperfect voltage divider and without total electrical isolation at the active region; therefore the injection current is the current supplied to the individual contact for that element, but not necessarily the total current injected into the element. In these measurements the array output beam is completely detected, regardless of coherent or incoherent operation. As depicted in Fig. 2(a), there is a significant difference in the output power and lasing threshold when each element is biased separately.

Furthermore the near-field shows lasing only in the biased array element, indicating electrical isolation between the elements of the array. Shown in Fig. 2(b) is the output power for a constant bias current I_2=4.1 mA applied to Element 2, while the current I_1 is varied to Element 1. Note the distinct increase in output power at I_1=3.6 and 4.4 mA in Fig. 2(b). We show below that these perturbations in the output power correspond to bias conditions at which we tune the resonance of Element 1 into optical coherence with Element 2.

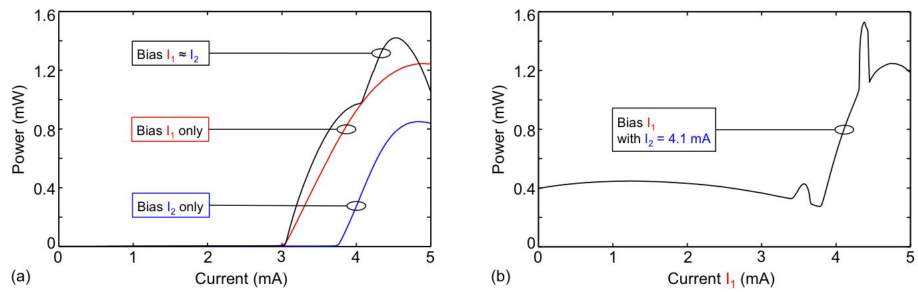

Figure 2. Output power vs. bias current for 2×1 array with varied bias applied to (a) Element 1 only (red), Element 2 only (blue), Elements 1 and 2 simultaneously (black), and (b) Element 1 with a constant current I_2=4.1 mA applied to Element 2 [11].

Resonance tuning into coherence for the array is explicitly demonstrated in Fig. 3. The spatially resolved peak wavelengths of the lasing modes of Elements 1 and 2 are shown in Fig. 3 for different biasing schemes. Fig. 3(a) shows constant bias current I_2=4.1 mA while I_1 is varied. Increasing the current injection into either array element increases (decreases) the cavity refractive index for that element through ohmic heating (electronic suppression) [8], thus varying its natural resonance wavelength. Ohmic heating and current spreading into the inter-element regions of the array influence the refractive index in that region as well, thus the index profile across the array is varied with current injection [11].

As depicted in Fig. 3(a), starting at a lower bias current and then increasing the current injection to Element 1 allows us to tune its cavity resonance to be shorter or longer with respect to the lasing wavelength of Element 2. As seen in the inset of Fig. 3(a), we find that over a range of approximately 100 μA around I_2=4.4 mA, the fundamental modes of both elements are locked at the same resonance frequency, becoming unlocked when the wavelength detuning between each cavity's fundamental mode resonance becomes greater than about 0.1 nm (±0.03 nm). The extent of this locking range while varying current injection into one of the elements, which in turn is related to an amount of frequency detuning allowed while the array remains locked in coherently coupled operation, varies between different array designs and for the same array under different bias conditions. It should be noted that there is often an observed hysteresis with this locking range, as it is noticeably made larger by first locking the elements of the array and then increasing the frequency detuning of the elements while locked in coherently coupled operation. As depicted in Fig. 2(b), the locked resonance wavelength is accompanied by a significant increase in the output power over this small range of injection currents, greater than is otherwise achieved [11]. Similar behavior is found for reversing these measurements with constant current I_1 and tuning the current injection to Element 2.

Coherence tuning is explicitly demonstrated in Fig. 3(b). The spatially resolved emission spectra and far-field intensity profile for the 2×1 array are shown in Fig. 3(b) for several bias conditions indicated by points α, β, and γ in Fig. 3(a). Notice that by electrically tuning the fundamental modes of Elements 1 and 2 into spectral overlap (region β in Fig. 3), the array becomes coherently coupled in an out-of-phase mode as indicated by an on-axis null in the far-field intensity profile. Moreover, with sufficient detuning (conditions α and γ in Fig. 3), two clearly defined spectral peaks with a single broad Gaussian far-field are apparent when Elements 1 and 2 are uncoupled and thus incoherent. We have found nearly every 2×1 array that has been tested and that is suitably designed [17] with sufficient electrical isolation can be tuned to operate in a regime of coherent coupling [11]. Hence, by independently varying the bias we can tune the resonance of each element and thus, for virtually all phased arrays, achieve variable phase and coherence of the array [11, 20, 21].

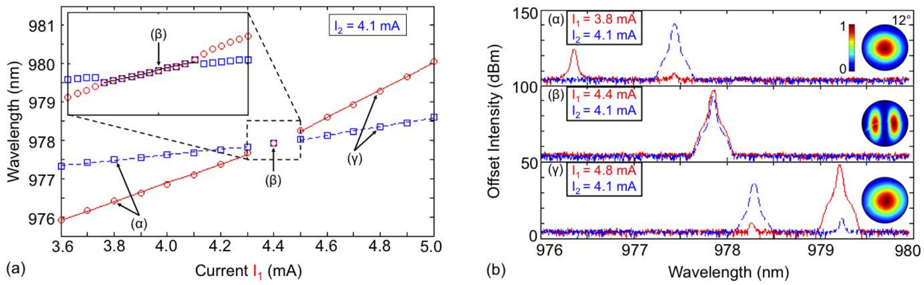

Figure 3. Spatially resolved spectral data showing fundamental mode wavelength vs. bias current for Elements 1 (red circle) and 2 (blue square) for (a) I_2=4.1 mA while I_1 is varied and (b) I_1=4.4 mA while I_2 is varied. Inset shows locking range. (b) Spatially resolved spectral data showing intensity vs. wavelength for Elements 1 (red solid) and 2 (blue dashed) corresponding to the three data points labeled in Fig. 3(a). Inset shows the corresponding far-field intensity profiles [11].

Coherently coupled operation does not require specific bias currents nor necessarily produce similar coupled mode behavior. Instead we find that any suitable array can be tuned to coherence at varying bias conditions, and, in many cases, be tuned to operate in both the in-phase and out-of-phase mode [11]. Note the power increase in Fig. 2(b) at I_1=3.6 and I_2=4.1 mA. This corresponds to a bias condition at which the Gaussian mode of Element 1 has been tuned into coherence with a higher order mode of Element 2. In this case we can achieve in-phase coupling, as shown by data from a similar 2×1 VCSEL array in Fig. 4.

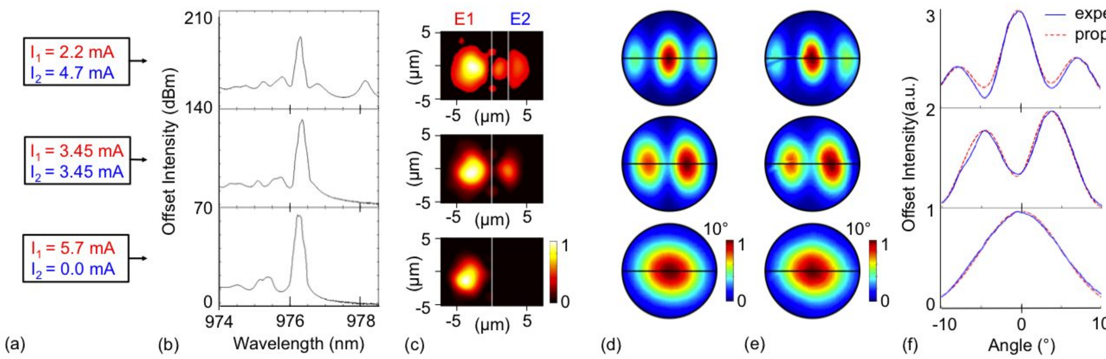

Figure 4. In-phase (top), out-of-phase (middle), and incoherent (bottom) operation of 2×1 VCSEL. The (a) bias conditions, (b) spectra, (c) processed near-field where white lines delineate the apertures used for simulation, (d) propagated far-field, and (e) experimental far-field for an array under varying current injection are shown; (f) far-field profiles are compared across the black lines shown in (d) and (e) [11].

Analysis of the near-field and far-field intensity profiles allows us to verify that the observations indicate coupled mode behavior and not the typical behavior of higher-order mode emission. For a similar 2×1 VCSEL array, regions of coherently coupled operation for both in-phase and out-of-phase coupled mode behavior are shown in Fig. 4 for equal total current injection and constant emission wavelength but with different bias conditions resulting in varying index profile across the array and spectral overlap of different cavity modes from each element. By propagating the near-field apertures to the far-field via the Fraunhofer approximation, we are able to closely match the behavior of the experimentally determined far-field intensity profile thereby extracting the phase difference and coupling efficiency of the laser array under these instances of coherently coupled operation [20]. As shown by Fig. 6, for bias currents I_1=2.2 mA and I_2=4.7 mA there is spectral overlap between the fundamental mode of Element 1 and higher-order modes of Element 2. This bias condition produces an in-phase coupled mode (with extracted phase difference of 13° between elements) as indicated by the near-field central lobe and on-axis narrow peak in the far-field intensity profile. For bias currents I_1= I_2=3.45 mA there is spectral overlap between the fundamental modes of both Elements 1 and 2. This bias condition produces an out-of-phase coupled mode (with extracted phase difference of 164° between elements) as indicated by the near-field central null and on-axis null in the far-field intensity profile. Note that the phase difference between coupled elements is not discrete but is continuously tuned about 0 (in-phase mode) and π (out-of-phase mode) with observed reduced coupling efficiency when the phase approaches ±π/2, consistent with previous work [21].

3. RESULTS

3.1 Modulation Response Enhancement

DC current injection into the array elements is achieved with high-precision current sources biasing the sample via a high-speed GSSG probe. The modulation response and optical spectra are simultaneously measured by use of a 1x2 fiber splitter, optical spectrum analyzer (OSA), high-speed photoreceiver with 25 GHz 3-dB bandwidth, and Agilent E8363C 40 GHz parameter network analyzer.

Fig. 5 shows the output power and voltage versus current for an array under different biasing schemes. The voltage versus current data has been included to allow for estimates of resistance, power efficiency and compatibility with high-speed driver circuits. As shown in Fig. 5(a), there is a difference in the output power for each element biased separately indicating significant electrical isolation between array elements. Near-field observation also confirmed for biasing up to 8 mA, only the biased array element lases. By electrically tuning Elements 1 and 2, we obtain highly single-mode emission with an out-of-phase mode throughout the coherent operation regime, one of which is apparent in Fig. 5(b) with 4.3 to 5.6 mA injected into Element 2. With sufficient detuning two clearly defined spectral peaks with a single broad Gaussian far-field are apparent when the elements become uncoupled and incoherent.

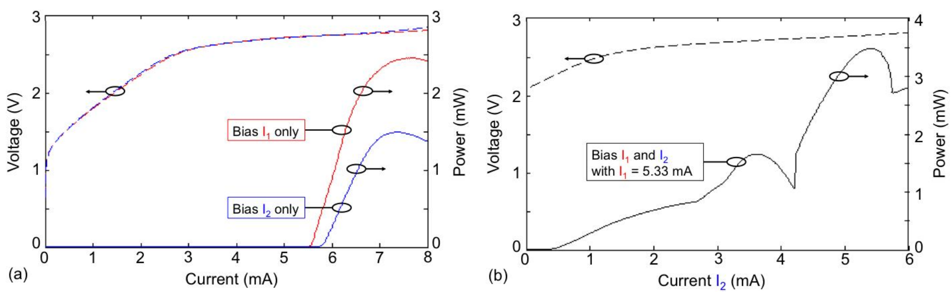

Figure 5. Output power and voltage vs. bias current for 2×1 array with varied bias applied to (a) Element 1 only (red), Element 2 only (blue), and (b) Element 2 with a constant current I_1=5.33 mA applied to Element 1 [10].

Fig. 6(a) shows the small signal modulation response of the 2x1 VCSEL array shown in Fig. 5. For reference the modulation response of a single element photonic crystal VCSEL from the same sample biased at I = 8 mA or about 4x threshold current is included in Fig. 6(a). The current applied to Element 1 is modulated with a constant DC bias I_1 = 5.33 mA (current resolution of ± 5 µA), while the DC bias, I_2, applied to Element 2 is varied in order to tune resonance and thus the phase relation and coupling between the two elements. For bias values of I_2 producing incoherent array operation, the modulation response of the 2x1 array is similar to that of an individual VCSEL. The maximum achieved 3-dB bandwidth is 37 GHz (limited by the photoreceiver bandwidth) obtained at injection currents of I_1=5.33 mA and I_2=5.44 mA. The simultaneously measured emission spectra for the 2x1 array while producing this modulation response behavior is shown in Fig. 6(b). For this condition, Elements 1 and 2 are coherently coupled with 40 dB SMSR and narrow RMS spectral width of 0.043 nm (calculated according to the IEEE 802.3 Standard) for the coupled mode. In the far-field we observe two lobes with an on-axis null in between them, indicating out-of-phase coupling. The bias currents corresponding to those giving the maximum enhanced bandwidth produce an output power of > 3.4 mW as shown in Fig. 5(b). The maximum enhanced bandwidth is achieved at an operating current density of < 8 kA/cm2 [10].

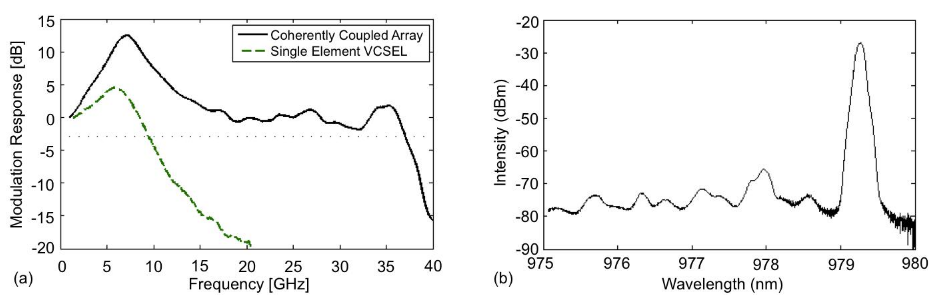

Figure 6. (a) Modulation response (black solid) and (b) spectra of the coherently coupled 2x1 VCSEL array under direct modulation with dc bias at I_1 = 5.33 mA and I_2 = 5.44 mA. In (a) the modulation response (green dashed) of a single element photonic crystal VCSEL from the same sample biased at I = 8 mA is included for comparison [10].

We have performed measurements on 2x1 arrays with different structural designs and from other epitaxial wafers for both 980 and 850 nm emission wavelengths [10]. The measured bandwidth enhancement beyond 30 GHz has been observed from several arrays. Similar improvements in bandwidth enhancement have been observed from arrays emitting nominally at the 850 nm wavelength. Inconsistent bandwidth enhancement of lesser magnitude has been observed to occur serendipitously from arrays without electrical isolation between elements (e.g. without the FIB etch), showing that while unnecessary for producing bandwidth enhancement, electrical isolation is essential for its control and optimization through resonance and coherence tuning. Furthermore, it has been observed that while the bandwidth enhancement correlates with spectral detuning of the natural resonances of array elements emitting in a coherently coupled mode, the phase and strength of the coherent coupling play a role in determining the frequencies of additional resonances and RF gain of those resonances in the modified modulation response [10].

The modulation response of multiple 2x1 phased photonic crystal VCSEL arrays with different device designs under varying bias conditions is shown in Fig. 7. An array can be tuned to produce an enhanced frequency response to better suit a specific application [12]. By controlling the electric field amplitude and phase being coupled between array elements through device design and bias conditions, we can engineer the device to achieve the modulation response desired for a particular application. Modulation bandwidths beyond 30GHz are particularly useful for ultra-fast optical interconnects in data center, server cluster, and supercomputer applications. A narrow bandwidth amplifier, centered at a millimeter-wave frequency, is useful for ultra-fast wireless communications and radio-frequency photonic-link technologies.

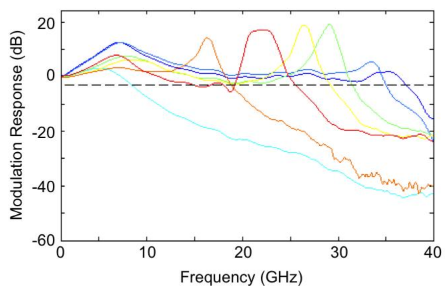

Figure 7. Modulation response of 2x1 VCSEL with several different device designs while biased within a coherently coupled locking range to produce enhanced resonance frequency. Bandwidth enhancement beyond 35 GHz is shown by the dark blue curve. Narrow-band enhanced modulation amplitudes, tuned to center frequencies between 15 and 30GHz, are shown by the orange, red, yellow, and green curves. For comparison, the modulation response of an array at bias conditions that do not produce coherent coupling is shown by the cyan curve.

4. ANALYSIS

4.1 Dynamic Coupled Mode Theory

In order to engineer an array for the desired behavior of a particular application, it is important to understand the theory that governs its dynamics. Coupled mode theory is only strictly valid for structures where the modes of individual lasing elements are well confined, as in guided coupling, and may not be the most suitable approach for examining the dynamics of antiguided VCSEL arrays. However, dynamic coupled mode theory is highly developed and has been successfully applied to coupled and injection-locked VCSEL arrays [22, 23]. The time change of the electric field of element m defined as $E_m = A_m\exp[-j\Phi_m(t)]$ where A_m is the field amplitude and Φ_m is the phase, under the influence of neighboring elements m+1 and m-1 is governed by the field and carrier equations [22],

$$\frac{dE_m(t)}{dt} = \frac{1}{2}\left[\Gamma g(t)(1-j\alpha) - \frac{1}{\tau_p}\right]E_m(t) + j\kappa\left[\left(E_{m+1}(t) + E_{m-1}(t)\right)\right]e^{-j\Psi} - j\left(\omega_m - \omega_0\right)E_m(t) + F_{sp} \tag{1}$$

and

$$\frac{dN_m(t)}{dt} = \frac{\eta_i}{qV}I(t) - \frac{N_m(t)}{\tau_c(t)} - \gamma g(t)\left|E_m(t)\right|^2 \tag{2}$$

with non-linear gain g(t), carrier density N_m, linewidth enhancement factor α, coupling rate coefficient κ, phase Ψ between elements (typically 0 or π), current injection efficiency η_i, confinement factor Γ, spontaneous emission term F_{sp}, current I(t), carrier-dependent carrier lifetime $\tau_c(t)$, and the natural resonance ω_m and coupled mode resonance ω_0 frequencies. Through rate-equation analysis with Equations 1 and 2, we simulate the locking-range map in Fig. 8 and the corresponding modulation responses in Fig. 9 for the effects of a single element on another, much like those for an injection locked laser [22-25]. Common device performance parameters for VCSELs were used in our simulations [26].

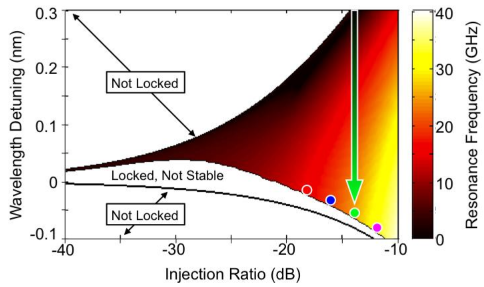

Figure 8. Simulated map of the locking range shows resonance frequency of modulation response vs. wavelength detuning and field injection ratio for one element with optical injection from another.

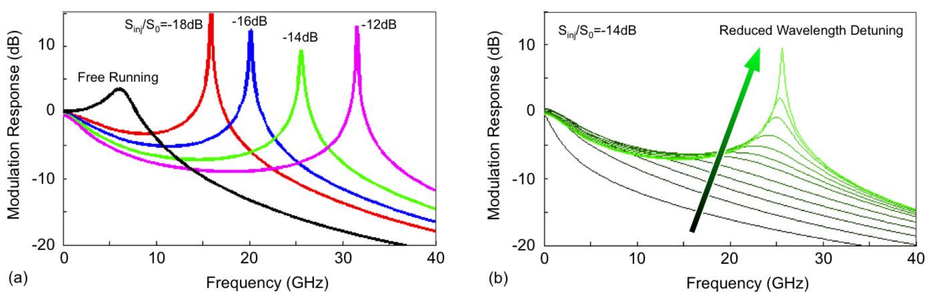

Figure 9. Simulated modulation response curves using Equations 1 and 2. Modulation response curves in (a) have phase relation corresponding to the low wavelength detuning edge of a locking range with varying amounts of field injection ratio corresponding to the map locations indicated in Fig. 8 with same color circles. Modulation response curves in (b) have the same injection ratio but with varying coherent coupling phase / spectral detuning between elements corresponding to the map locations indicated in Fig. 8 with same color arrow.

The locking range map in Fig. 8 shows the resonance frequency of modulation response vs. wavelength detuning and injection ratio for one element being coupled to another. The wavelength detuning is that between the natural resonance of laser array element m, λ_m, and the coupled mode resonance of the coherently coupled laser array, $\lambda_{coupled}$. The injection ratio or coupling ratio, defined as $A_{coupled}^2/A_m^2$, is the ratio of the magnitude of field amplitude being injected or coupled from a neighboring laser array element, $A_{coupled}^2$, with respect to that of the free-running laser array element m being injected, A_m^2. The resonance frequency of modulation response is given by

$$\omega_{res}^{\ 2} = \left| \kappa \frac{A_{coupled}}{A_0} \sin \Phi_m \right| + \omega_{OR}^{\ 2} \tag{3}$$

where ω_{OR} is the modulation response resonance frequency due to relaxation oscillation for the free-running laser array element m. The locking range map in Fig. 8 is useful when determining bias points to induce a desired modulation response. Along with Fig. 9(a), it shows the general trend that increasing the injection ratio increases the resonance frequency. It also shows that the modulation bandwidth is not proportional to the resonance frequency as there is a dip that occurs between DC and the resonance frequency, thereby reducing the usable broadband frequency range. Along with Fig. 9(b), it shows that at positive wavelength detuning the response has high gain but low bandwidth whereas a sharp and high frequency resonance peak is induced by zero / negative wavelength detuning. Preliminary analysis of the behavior from 2x1 arrays as a monolithic injection locked laser system using dynamic coupled mode theory has been reported [15]. Modeling the response of both elements under the simultaneous influence of each other with experimental analysis of the spectral detuning, coherence phase, and coherence magnitude will be reported in another publication.

5. CONCLUSIONS

In conclusion, we show that by resonance tuning of properly designed 2×1 optically coupled phased VCSEL arrays, we can achieve coherently coupled operation at various bias conditions [11]. This control ensures coherently coupled operation from nearly all arrays and provides access to significantly increased output power as well as either in-phase or out-of-phase coherent operation [11], by which we may take advantage of beneficial properties depending on the application [10, 19]. This ability to tune into coherence will enhance the performance of phased vertical cavity laser arrays as well as improve their fabrication yield. We demonstrate that resonance detuning and variation of the phase relation and coherence of 2x1 photonic crystal VCSEL arrays can simultaneously achieve enhanced modulation response with narrow single-mode spectral width and relatively high output power while operating at low current density, all of which are desirable for reliable data transmission over large distances in fiber [10]. Larger arrays with different phase relationships between elements also could potentially allow for increased output power and further manipulation of the modulation response with more resonance frequencies and increased RF gain, thus further enhancing modulation bandwidth. By applying dynamic coupled mode theory to the analysis of phased, photonic crystal VCSEL arrays under coherently coupled operation, we are able to gain insight to the modulation response and locking range dynamics observed experimentally. This analysis may improve our understanding and ability to engineer laser arrays for a number of applications.

REFERENCES

[1] Tatum, J. A., "Evolution of VCSELs," Proc. SPIE OPTO, 90010C-90010C-9 (2014).

[2] Kuchta, D., Rylyakov, A. V., Schow, C. L., Proesel, J., Baks, C., Westbergh, P., Gustavsson, J. S., and Larsson, A., "64Gb/s Transmission over 57m MMF using an NRZ Modulated 850nm VCSEL," Optical Fiber Communication Conference, Th3C. 2 (2014).

[3] Westbergh, P., Haglund, E., Haglund, E., Safaisini, R., Gustavsson, J. S., and Larsson, A., "High-speed 850 nm VCSELs operating error free up to 57 Gbit/s," Electron.Lett. 49(16), 1021-1023 (2013).

[4] Tan, M. P., Fryslie, S. T. M., Lott, J., Ledentsov, N., Bimberg, D. and Choquette, K. D., "Error-free transmission Over 1-km OM4 multimode fiber at 25 Gb/s using a single mode photonic crystal vertical-cavity surface-emitting laser," Photonics Technology Letters, IEEE 25(18), 1823-1825 (2013).

[5] Safaisini, R., Haglund, E., Westbergh, P., Gustavsson, J. S., and Larsson, A., "20 Gbit/s data transmission over 2 km multimode fibre using 850 nm mode filter VCSEL," Electron.Lett. 50(1), 40-42 (2014).

[6] Grabherr, M., Jager, R., Michalzik, R., Weigl, B., Reiner, G., and Ebeling, K., "Efficient single-mode oxide-confined GaAs VCSEL's emitting in the 850-nm wavelength regime," Photonics Technology Letters, IEEE 9(10), 1304-1306 (1997).

[7] Choquette, K. D., Siriani, D. F., Kasten, A. M., Tan, M. P., Sulkin, J. D., Leisher, P. O., Raftery, J. J., and Danner, A. J., "Single mode photonic crystal vertical cavity surface emitting lasers," Advances in Optical Technologies 2012 (2012).

[8] Siriani, D. F., and Choquette, K. D., "Implant defined anti-guided vertical-cavity surface-emitting laser arrays," Quantum Electronics, IEEE Journal of 47(2), 160-164 (2011).

[9] Dalir, H., and Koyama, F., "29 GHz directly modulated 980 nm vertical-cavity surface emitting lasers with bow-tie shape transverse coupled cavity," Appl. Phys. Lett. 103(9), 091109 (2013).

[10] Fryslie, S. T. M., Tan, M. P., Siriani, D. F., Johnson, M. T., and Choquette, K. D., "37-GHz modulation via resonance tuning in single-mode coherent vertical-cavity laser arrays," Photonics Technology Letters, IEEE 27(4), 415-418 (2015).

[11] Fryslie, S. T. M., Johnson, M. T., and Choquette, K. D., "Coherence tuning in optically coupled phased vertical cavity laser arrays," Quantum Electronics, IEEE Journal of 51(11), 1-6 (2015).

[12] Fryslie, S. T. M., and Choquette, K. D., "Optoelectronics & Communications Coherently coupled laser arrays for low-dispersion, ultra-high-bandwidth data transfer," SPIE Newsroom, 10.1117/2.1201505.005958 (2015).

[13] Fryslie, S. T. M., and Choquette, K. D., "Breakthroughs in Photonics 2014: Coherent Vertical-Cavity Surface-Emitting Laser Arrays," Photonics Journal, IEEE 7(3), 1-5 (2015).

[14] Hawkins, B., Hawthorne III, R. A., Guenter, J. K., Tatum, J. A., and Biard, J., "Reliability of various size oxide aperture VCSELs," Electronic Components and Technology Conference, 2002. Proceedings. 52nd, 540-550 (2002).

[15] Fryslie, S. T. M., and Choquette, K. D., "Analysis of modulation response and locking range dynamics for coherently coupled phased, vertical cavity laser arrays," IEEE Photonics Conference, 591-592 (2015).

[16] Raftery, J. J., Danner, A. J., Lee, J. C., and Choquette, K. D., "Coherent coupling of two-dimensional arrays of defect cavities in photonic crystal vertical cavity surface-emitting lasers," Applied Physics Letters 86(20), 201104 (2005).

[17] Siriani, D. F., Leisher, P. O., and Choquette, K. D., "Loss-induced confinement in photonic crystal vertical-cavity surface-emitting lasers," Quantum Electronics, IEEE Journal of 45(7), 762-768 (2009).

[18] Lehman, A. C., and Choquette, K. D., "One-and two-dimensional coherently coupled implant-defined vertical-cavity laser arrays," Photonics Technology Letters, IEEE 19(19), 1421-1423 (2007).

[19] Johnson, M. T., Siriani, D. F., Tan, M. P., and Choquette, K. D., "High-speed beam steering with phased vertical cavity laser arrays," Selected Topics in Quantum Electronics, IEEE Journal of 19(4), 1701006-1701006 (2013).

[20] Johnson, M. T., Siriani, D. F., Sulkin, J. D., and Choquette, K. D., "Phase and coherence extraction from a phased vertical cavity laser array," Applied Physics Letters 101(3), 031116 (2012).

[21] Johnson, M. T., Siriani, D. F., Tan, M. P., and Choquette, K. D., "Beam steering via resonance detuning in coherently coupled vertical cavity laser arrays," Applied Physics Letters 103(20), 201115 (2013).

[22] Lang, R., "Injection locking properties of a semiconductor laser," Quantum Electronics, IEEE Journal of 18(6), 976-983 (1982).

[23] Wang, S. and Winful, H., "Dynamics of phase-locked semiconductor laser arrays," Applied Physics Letters 52(21), 1774-1776 (1988).

[24] Simpson, T., Liu, J., Gavrielides, A., Kovanis, V., and Alsing, P., "Period-doubling route to chaos in a semiconductor laser subject to optical injection," Applied Physics Letters 64(26), 3539-3541 (1994).

[25] Mogensen, F., Olesen, H., and Jacobsen, G., "Locking conditions and stability properties for a semiconductor laser with external light injection," Quantum Electronics, IEEE Journal of 21(7), 784-793 (1985).

[26] Coldren, L. A., Corzine, S. W., and Mashanovitch, M. L., [Diode Lasers and Photonic Integrated Circuits], John Wiley & Sons (2012).